Mixed selectivity coding of content-temporal detail by dorsomedial posterior parietal neurons

Lei Wang[1,2,3], Xufeng Zhou[1], Jie Yang[1], Fu Zeng[3], Shuzhen Zuo[1], Makoto Kusunoki[4,5], Huimin Wang[1,3,6,7], Yong-di Zhou[8], Aihua Chen[3], Sze Chai Kwok[1,2,3,6,7,9]

1. Shanghai Key Laboratory of Brain Functional Genomics, Affiliated Mental Health Center (ECNU), School of Psychology and Cognitive Science, East China Normal University, Shanghai, China
2. Division of Natural and Applied Sciences, Duke Kunshan University, Duke Institute for Brain Sciences, Kunshan, Jiangsu, China
3. Key Laboratory of Brain Functional Genomics (Ministry of Education), East China Normal University, Shanghai, China
4. MRC Cognition and Brain Sciences Unit, Cambridge, UK
5. Department of Experimental Psychology, University of Oxford, UK
6. Shanghai Key Laboratory of Magnetic Resonance, East China Normal University, Shanghai, China
7. Shanghai Changning Mental Health Center, China
8. School of Psychology, Shenzhen University, Shenzhen, China
9. Lead contact

Corresponding author: sze-chai.kwok@st-hughs.oxon.org

HIGHLIGHTS

- Neural codes for "neuroethogram" in macaque dorsomedial parietal cortex
- Parietal neural codes exhibit mixed selectivity of event features
- Dorsomedial PPC neurons support a long temporal receptive window for episodes

SUMMARY

The dorsomedial posterior parietal cortex is part of a higher-cognition network implicated in elaborate processes underpinning memory formation, recollection, episodes reconstruction, and temporal processing. Neural coding for complex episodic processing is however largely undocumented. Here we revealed a set of neural codes of "neuroethogram" in the primate parietal cortex. Analyzing neural responses in macaque dmPPC to naturalistic videos, we discovered several groups of neurons that are sensitive to categories of ethogram-items and to low-level sensory features. The amount of information coded within these multiplex representations in turn increases our trained classifier decodability for different video-types. We further discovered that the processing of category and feature information by these neurons is sustained by accumulation of temporal information over a long timescale, corroborating its role at the apex of the cortical hierarchy of temporal receptive windows. Taken altogether, these neural findings explain how dorsomedial PPC weaves fabrics of ongoing experiences together in real-time and realize a multiplex representation of an organism's past. The high dimensionality of neural representations should motivate us to shift the focus of attention from pure selectivity neurons to mixed selectivity neurons, especially in increasingly complex naturalistic task designs.

KEYWORDS

Neuroethology, dorsomedial posterior parietal cortex, information accumulation, temporal receptive window, mixed selective representation

INTRODUCTION

In an ever-changing environment, massive amounts of multidimensional information embedded in continuous events rushes into the cognitive system. The neural system has to extract pieces of meaningful information, integrate, and encode them into memory systems in time for future needs. The dorsomedial posterior parietal cortex (dmPPC), which consists of the paracentral Area 7 and precuneus (Cavanna & Trimble, 2006), is part of the posterior-medial memory system (Ranganath & Ritchey, 2012) and has strong and wide-spread anatomical connections with its adjacent structures, including the early visual cortex, sensorimotor regions, medial temporal areas, and prefrontal cortex in both macaque monkeys and humans (Cavanna & Trimble, 2006; Kravitz et al., 2011; Morecraft et al., 2004).

A wealth of studies demonstrated that the dmPPC plays critical roles in multifaceted cognitive processes, including visual-spatial attention and locomotion processes in egocentric environment (Bartels et al., 2008; Ghaem et al., 1997), sensorimotor transformation processes, such as object manipulation (Gardner et al., 2007), execution and observation of reaching-to-grasp behaviors (Evangeliou et al., 2009), representations of enumeration (Harvey et al., 2013), decision making (Hutchinson et al., 2015; Murray et al., 2017), self-related processing (Cavanna & Trimble, 2006), and episodic memory formation and retrieval (Brodt et al., 2018; Brodt et al., 2016). The dmPPC is part of an integral hub for extracting and scaffolding information in real-time from the environment (Reagh & Ranganath, 2021) as well as with other agents (Freedman & Ibos, 2018; Kravitz et al., 2011).

Given the region's myriad functions, the conventional logic of stimulus-response models might not be adequate for studying neuronal responses to complex stimuli and their interactions. For example, neurons in high-order brain areas especially in associative areas, such as the prefrontal cortex (Rigotti et al., 2013) could show mixed selectivity properties to different stimuli (Fusi et al., 2016; Wallach et al., 2021). Recently, Platt and his colleagues confirmed that neurons in PFC and OFC were engaged in valuing social information with a measure known as "neuroethogram" (Adams et al., 2021). A neuroethogram is defined as fitting neural activities to dimensional ethograms, which is a technique for annotating species-typical behavior frame-by-frame. Considering that the primate Area 7 is part of a social interaction network (Sliwa & Freiwald, 2017) and a posterior-medial memory network (Ranganath & Ritchey, 2012), we predict that dmPPC neurons process information embedded within complex behaviorally meaningful events in a multiplex manner.

In addition to leveraging on multifunctional features contained in naturalistic videos, we were mindful that temporal information is another fundamental aspect of events (Clewett et al., 2019). Since information is carried out over distinct timescales, we know that the ability of information accumulation changes from the primary sensory cortex to the high-order cortex (Hasson et al., 2015; Hasson et al., 2008). These studies propose that brain areas are organized with hierarchical time receptive windows (TRW) so that brain regions with long TRW will accumulate transient sensory signals from short TRW brain areas for flexible processing. The primate precuneus plays an essential role in temporal information processing (Murray et al., 2014) involved in time estimation (Onoe et al., 2001) and temporal information integration of movies of up to 12 s (Andric et al., 2016; Hasson et al., 2008). It is unclear how neurons in the dmPPC might dynamically assemble such temporal details to support such episode processing.

To address these two issues on processing multiplex content and passage of time, we combined an ethogram methodology with dynamic cinematic material, together with multi-unit extracellular electrophysiology in awake macaque monkeys, to elucidate how dmPPC neurons process mixed selectivity representation of naturalistic content over time.

RESULTS

To study mixed selectivity coding, we had 3 monkeys view 18 different movies (categorically into Primate/Non-Primate/Scenery content-type) while we performed extracellular action potential recording on their dorsomedial posterior parietal cortex. On each day, the monkeys watched 3 different movies, each for 30 repetitions. These movies were custom edited to contain both content and temporal information (Figure 1A; Table S1). In total, we recorded extracellular activities of 375 units (monkey J: 164; monkey M: 157; monkey G: 54) (Figure 1B, Figure S1; STAR Methods; Movie S1).

Classification of neurons by their specificity to video's content-type.

By comparing the neural spiking rates to each of the three video content types, we observed that 33.07% (124/375) of the neurons exhibited significant (one-way ANOVA, Ps < 0.05) content-sensitive activity in the videos (Figure 1C-H), while 66.93% (251/375) showed no difference on firing rate across video contents (content-insensitive, Figure 1I). Among these content-sensitive neurons, 52.4% (65/124) of the units had a higher mean firing rate for Primate videos (Primate), whereas 8.9% (11/124) and 16.9% (21/124) had a higher mean firing rate to Non-primate (Non-primate) and Scenery (Scenery) videos, respectively (Figure 1C-E). In contrast, 10.5% (13/124) of these content-sensitive neurons discharged less to Primate videos (Non-primate-Scenery, Figure 1F), and 3.2% (4/124) and 8.1% (10/124) discharged less to Non-primate (Primate-Scenery, Figure 1G) and Scenery contents (Primate-Non-primate, Figure 1H). We found that the dorsomedial parietal neurons respond differentially to different video content-types, with some of them to the primate content, which is consistent with previous findings that a portion of this part of the monkey medial parietal cortex is activated by social interaction of conspecifics (Sliwa & Freiwald, 2017).

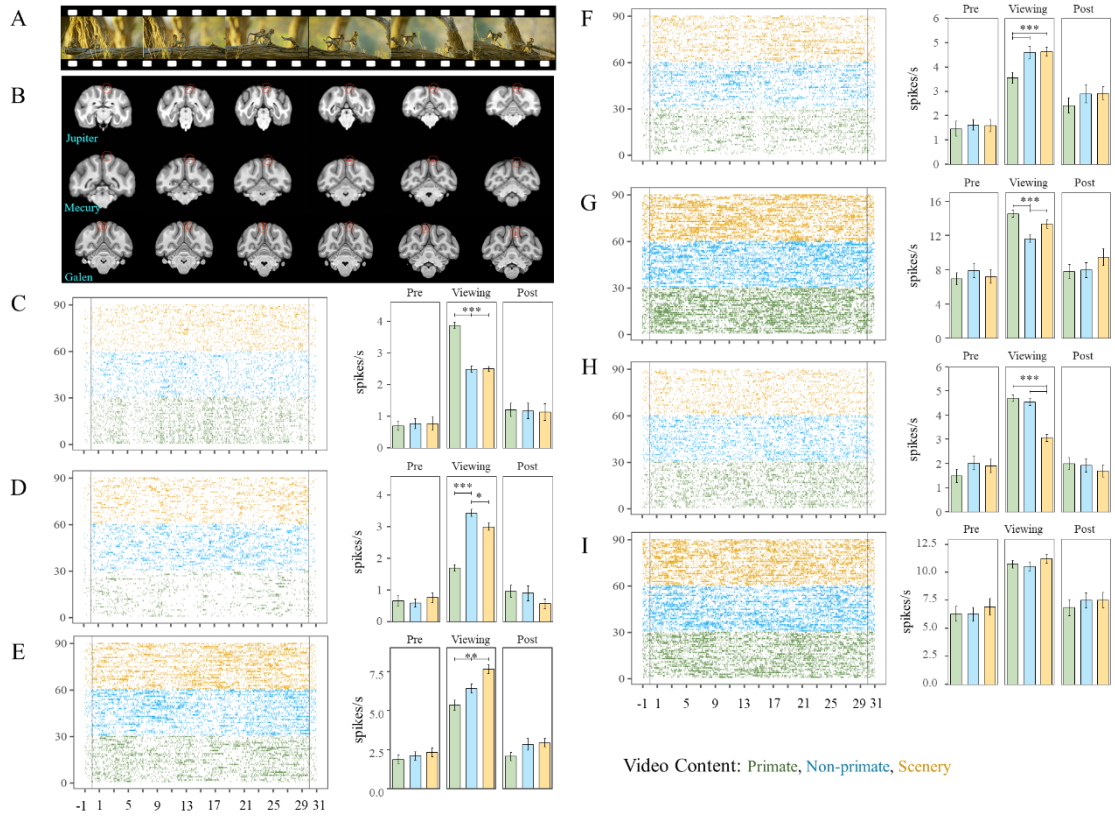

Figure 1. Experimental procedure, recording sites, and neuron classification. (A) Example video (a Primate-video) used in the study. Each day, the monkeys watched three different 30-s videos, each for 30 repetitions in 6 blocks; (B) Reconstruction of recording sites (circled in red) overlaid on T1 images; (C-I) Raster plots (left panels) and firing rate comparisons (right panels)

of 7 representative neurons responding to different video content-types. All show a significantly higher firing rate during video viewing than pre/before and post/after video presentation (Ps < 0.05). In raster plots, the X-axis indicates the time course of the video, and vertical lines represent the onset or offset of video display; each row is associated with a trial. Trials are re-ranked by video content-types (yellow: Scenery, blue: Non-primate, green: Primate). Three example content-sensitive neurons showed significantly higher firing rates to primate (C:#PC0056, Primate), non-primate (D:#PC0040, Non-primate), and scenery (E:#PC0114, Scenery) content-type. Firing rates of three content-sensitive neurons exhibited the lowest activity to primate (F:#PC0232, Non-primate-Scenery), non-primate (G:#PC0205, Primate-Scenery), and scenery (H:#PC0249, Primate-Non-primate) content-types. (I) A Content Insensitive example neuron (#PC0192) exhibited equal firing rates across different video content-types. Error bars: SEM. * P < 0.05, ** P < 0.01, *** P < 0.001.

Multiplex representation of ethogram-items and low-level features in dmPPC neurons.

We analyzed the videos in detail by employing a frame-by-frame annotation of ethogram schema, which contains a subset of binary time series of multiple social behaviors and non-social events for each video (Adams et al., 2021). To investigate how individual neuron encodes the dimensions of informative dynamic natural context, we fit a LASSO elastic network regulation regression for each neuron to fit the averaged single neural activities with the binary labeling of the 52 ethogram-items (Table S2) and four low-level visual features (Figure S2). The analysis produced a collection of non-zero coefficients. As shown with an example neuron, the model with the lowest mean squared error would be chosen (Figure S3A-C). We then validated the chosen model by demonstrating a significant relationship with the predicted neural firing rates ($F(1, 450) = 121.5$, $R^2 = 0.213$, $P < 10^{-5}$; Figure S3D). By applying this feature selection procedure for all neurons, our model indicated that the activity of a large percentage of neurons would either positively or negatively be influenced by a number of ethogram-items depicted in the videos (range from 3.73% to 74.13%; Figure 2A-B). The proportion of the neurons modulated by each of the features are higher than chance (see STAR Methods Chi-squared Simulation) (Figure 2). For example, the category "camera movement" including multiple camera motions modulate the discharge of about 83.20% (312/375) percentage of all units (Figure 3C). The category "count", that is the number of animals visible, influenced a significant portion of all units (92.27% (346/375), Figure 3C).

A large proportion of units respond to facial (visible face: 57.87%; side face: 47.47%; direct face: 74.13%; eye contact: 60.27%) and genital (visible genitals: 57.60%; prominent genitals: 53.87%; male genitals: 33.07%; female genitals: 22.4%) features (Figure 2A-B). With some particularly prominent ethogram-items, we ran one-sample t-tests to test for their modulatory effects. The results revealed that eye contact ($t(225) = 2.921$, $P = 0.004$, Cohen's $d = 0.194$), prominent genitals ($t(201) = 2.249$, $P = 0.026$, Cohen's $d = 0.158$), holding food in mouth ($t(132) = 2.298$, $P = 0.023$, Cohen's $d = 0.199$), allogroom ($t(43) = 2.561$, $P = 0.014$, Cohen's $d = 0.386$), mounted threaten ($t(48) = 2.911$, $P = 0.005$, Cohen's $d = 0.416$), and mutual aggression ($t(13) = 2.643$, $P = 0.020$, Cohen's $d = 0.706$) significantly enhanced neuron firing rates, whereas holding food ($t(50) = -2.750$, $P = 0.008$, Cohen's $d = 0.385$) reduced neuron activities (Figure 2C). By factoring in a detailed classification of spiking selectivity to video content, we divided all the neurons into 7 types according to their responses to content-types. We found an even more refined pattern for the corresponding results for these 7 types of neurons (Figure S4).

We also checked whether dmPPC neurons would play a role in the processing of low-level features (cf. monkey early visual cortex in (Russ & Leopold, 2015)). In the same LASSO model, low-level features tuned a very large proportion of the dmPPC neuronal responses ("low level features" in Figure 2A & dark red bars in 2B). A large subset of neurons was tuned by luminance (70.40%, 264/375), contrast (73.07%, 274/375), saturation (72.00%, 270/375), and optical flow (73.60%, 276/375) respectively. Considering it with the more detailed neuron types,

we found an even more refined pattern for the corresponding results (Figure S4).

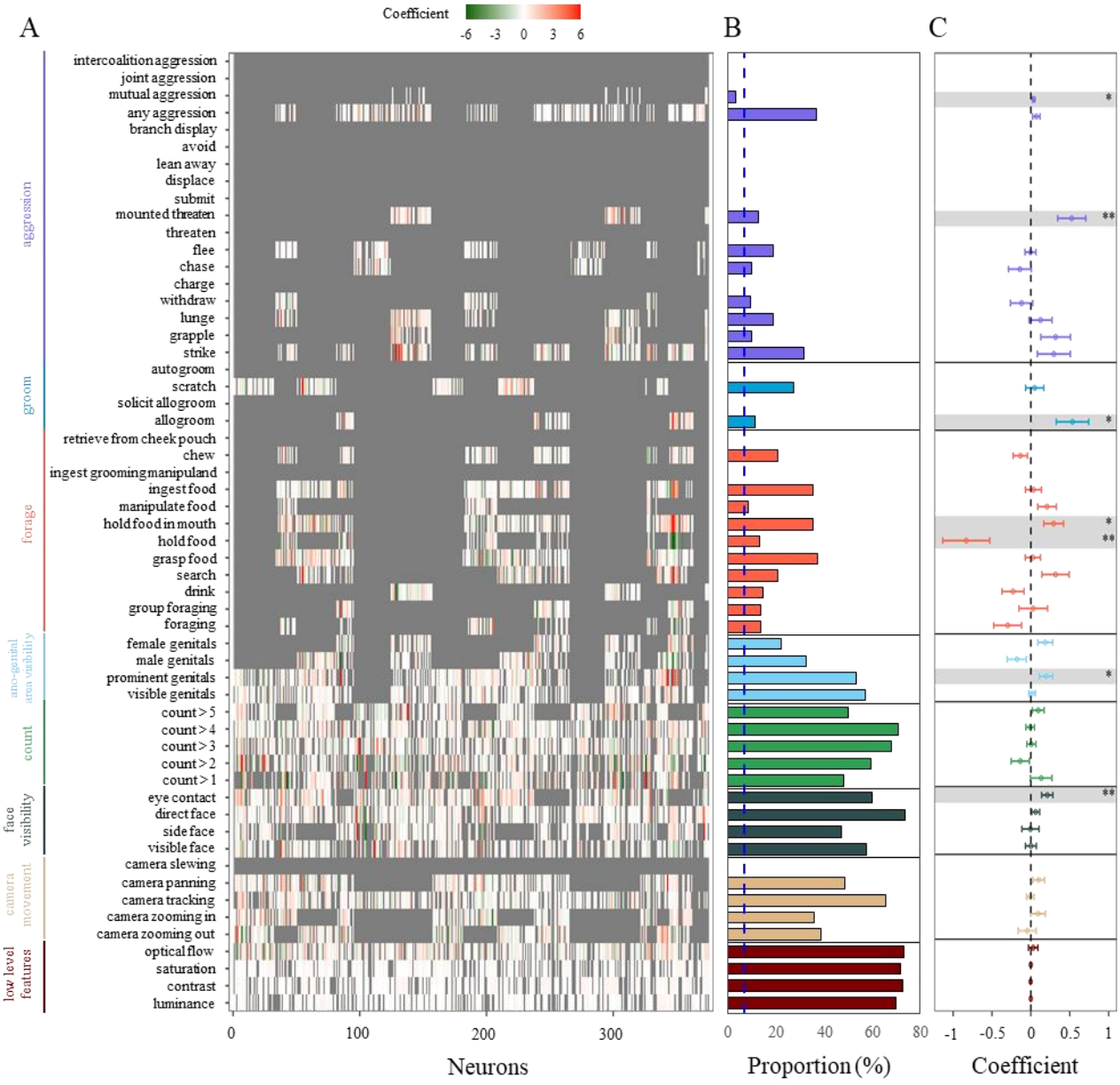

Figure 2. dmPPC neurons respond to social and non-social events in videos. (A) Effects of neuronal responses to 4 low level features (dark red) and 52 ethogram-items (seven categories of the ethogram organized by 7 different colors) obtained by a least absolute shrinkage and selection operator (LASSO) regression analysis. Each row stands for an item out of all 56 items, while each column refers to one neuron. (B) Proportion of neurons responsive to each item. (C) LASSO coefficient for each item tested against zero. Error bars: SEM. * $P < 0.05$, ** $P < 0.01$, *** $P < 0.001$.

To reflect this multiplex nature, we performed an intersection analysis and found that almost all (94.4%; 354/375) units showed mixed selectivity representations to at least three ethogram categories, 1.6% (6/375) neurons modulated by the combination of two ethogram categories, and only 4% (15/375) units selectively respond to one single ethogram category (Figure 3 & Movie S2).

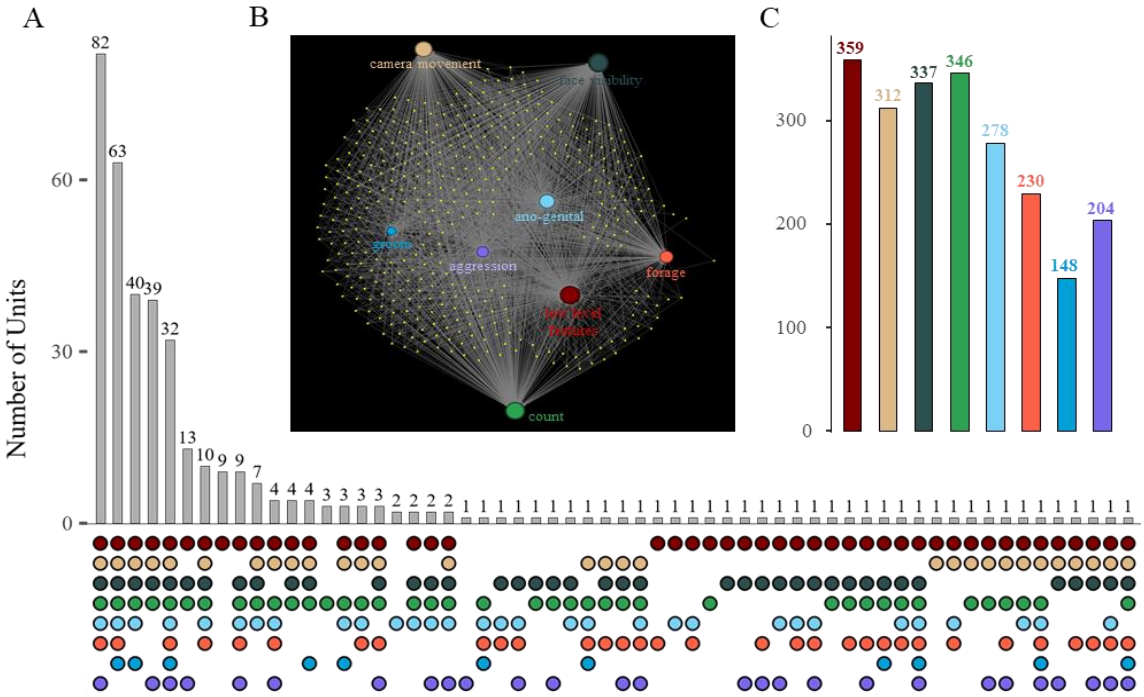

Figure 3. dmPPC neurons demonstrate mixed selectivity representations. (A) Distribution of neurons and their composition for mixed selectivity representations. Gray bars show the numbers of units exclusively modulated by combinations of mixed ethogram features, with their composition shown in the bottom panel. (B) Demonstration for dmPPC cell ensembles for their mixed selectivity coding. Each small yellow dot denotes a neuron. The eight circles with labels refer to the eight feature categories (low-level features and 7 ethogram categories), with their size proportional to the number of neurons modulated by that category. The connecting lines refer to the relationship between neurons and feature categories. See also an interactive illustration of the multiplex behavior of individual neurons on www.kwoklab.org. (C) Number of neurons that responded to each of the ethogram categories. Color coding here is the same as Figure 2 and Figure 3B.

Information coded for multiplex representation of features increases decodability for video content-types.

To examine whether and to what extent the temporal spiking patterns during viewing can differentiate the representations of categorical content, we trained a linear multiclass support vector machine (SVM) classifier with firing rate within 1-s time bins using a leave-one-out cross-validation approach for each neuron (see STAR Methods Content Discriminability). Overall, 40.80% (153/375) of the neurons exhibited a significant decoding ability when compared to a label-shuffled permutation statistical threshold (valid neurons, Ps < 0.05), while 59.20% (222/375) of the neurons showed insignificant decoding performance (invalid neurons, Ps > 0.05).

We then verified the multiplex representation of ethogram-items results with their relationship with decoded discriminability for each of the video's content-type. The group of neurons which produce a significant decoding accuracy per video content-type implicated significantly more selected features ($t(373) = 6.125$, $P < 0.001$, Cohen's $d = 0.644$; Figure 4A). A GLM regression revealed that the decoding accuracy of the valid decoder neurons was also significantly correlated with the number of selected features ($R^2 = 0.037$, $P < 0.017$; Figure 4B). On an individual neuron level, we found that neurons increased their decoding ability with the number of selected features for the Primate videos ($R^2 = 0.103$, $P < 5 \times 10^{-5}$; left panel in Figure 4C) but not for the Non-primate ($R^2 = 0.005$, $P = 0.374$) or Scenery videos ($R^2 = 0.002$, $P = 0.610$; Figure 4C). Specifically for Primate videos, when we considered the 8 regressors (7 ethogram-

items categories and 1 low-level category) separately, the relationship between decoding ability with the number of selected features was not present any more ($F(8,144) = 1.471$, $R^2 = 0.076$, $P = 0.173$), confirming a multiplex representation of features.

We observed that the percentages of neurons modulated for each selected feature were similar between valid and invalid decoding groups (Chi-square test: Ps > 0.8; Figure S5). LASSO coefficients are stronger in the valid decoder neurons for items carrying social information (e.g., "prominent genitals", "allogroom", and "flee"; Ps < 0.05; Figure S6C-D), but not for less social items such as "camera tracking" (Figure S6A) and "count" of animals (count > 1; Figure S6B). These results support the hypothesis that dmPPC neurons are implicated in episode processing for rich, naturalistic details.

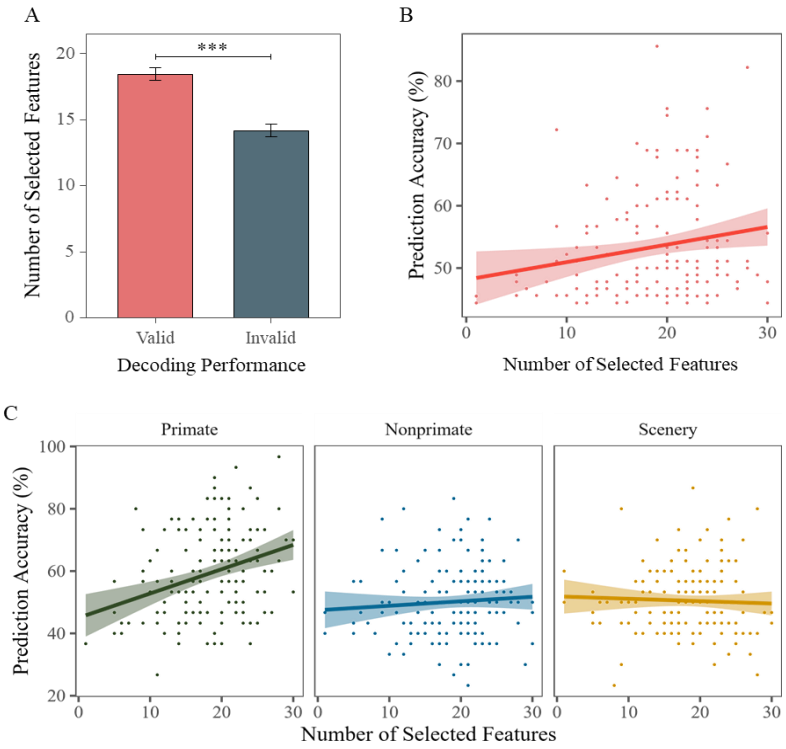

Figure 4. Relationship between mixed selectivity representation and individual neuronal decoding performance. (A) Neurons with valid decoding performance (greater than chance level, valid neurons) implicated more features than those neurons at chance level decoding performance (invalid neurons). (B) The number of selected features was significantly related to individual neuron's overall content-type discriminability (C) This relationship is significant for primate video content (left panel) but not for non-primate (middle panel) or scenery (right panel) video content-type. Lines represent linear regression of valid neurons. Dots refer to valid neurons. Error bars: SEM. *** $P < 0.001$.

Long temporal receptive window sustained by dmPPC neurons.

In light of the proposal that the parietal association cortex exhibits information accumulation over long timescale (Honey et al., 2012; Murray et al., 2014; Runyan et al., 2017), we hypothesized that the dmPPC cells might help scaffold the dynamic events temporally. To test this hypothesis, we constructed a multiclass SVM classier with stepwise accumulated sequential spiking using 1-s time bins across the videos (light green dots/line in Figure 5A; see STAR Methods Temporal Accumulation). Here, for this example neuron (*#PC0361*), we showed that accumulated 1-s epoch decoding produced a significantly better decoding performance than shuffled data ($t(29) = 11.013$, $P < 0.001$, Cohen's $d = 2.011$; dark green dots/line in Figure 5A), with prediction accuracy increased as a function of accumulated time

points (R^2 = 0.757, P < 10^{-5}). Moreover, for statistical inference, an identical SVM decoding procedure was applied but using neural activity for each 1-s time bin independently (yellow dots/line in Figure 5A). We ascertained that the prediction accuracy was not better than the permuted chance level (t(29) = -5.285, P < 0.001, Cohen's d = -0.965; slope not different from zero: R^2 = 0.006, P = 0.689; dark red in dots/line in Figure 5A). Planned paired t-tests confirmed that evidence accumulation is inherent in the temporal sequences rather than the single moments during which neurons fire (t(29) = 12.154, P < 0.001, Cohen's d = 2.219).

On a population level, 37.25% (57/153) of the neurons showed statistically significant information accumulation throughout the time course of videos. To assess the strength of the information accumulation, we compared the slopes by crossing two factors, Sequence (Accumulative/Individual) × Approach (Real/Shuffle) and found a two-way interaction (F(1,56) = 339.307, P < 10^{-5}, η2 = 0.531). These effects were derived from the stronger effects in accumulated real firing sequences than momentary neural firing (Real-Accumulated vs. Real-Individual: t = 25.603, P < 10^{-5}, Cohen's D= 2.919; left panel in Figure 5B) and no differences between the two shuffled conditions point (t = 0.645, P = 0.520; right panel in Figure 5B). These findings show that dmPPC neurons accumulate information of dynamic events in a progressively additive manner over the course of video viewing.

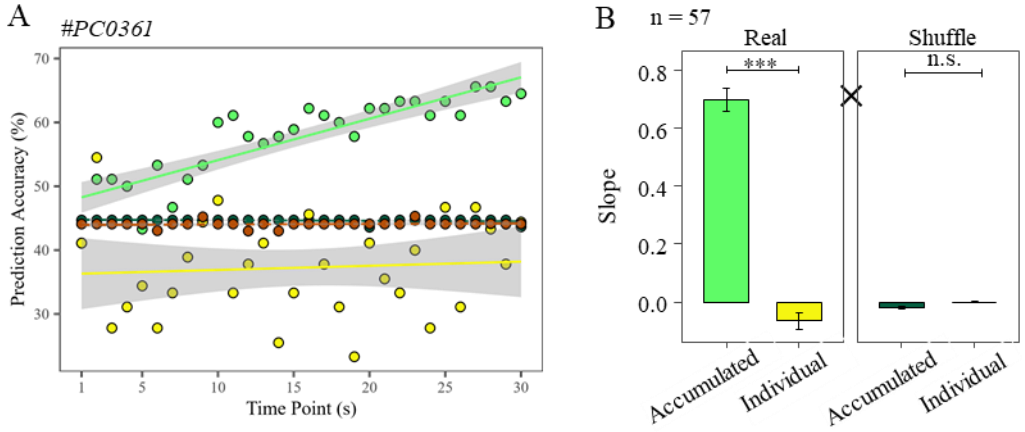

Figure 5. dmPPC neurons accumulate temporal evidence with long temporal receptive windows. (A) The decoding performance of the example neuron (#PC0361) positively correlates with cumulative spiking sequences (light green) but not with momentary neural activity (yellow). We used two sets of SVM decoding exercises to verify this property. First, we used cumulative spikes in 1-s time bins for 1st to 30th timepoint (accumulated sequence; light green) and compared it to chance level (dark green). Second, we used spikes in each individual time-point (yellow) and compared it with chance level (dark red). The four lines represent linear regression for these four SVMs for an example neuron. The dots refer to decoding performance of each timepoint. (B) A Sequence (Accumulative/Individual) × Approach (Real/Shuffle) two-way ANOVA revealed that the mean slope of population neurons (n = 57) was higher for real and cumulative sequences than for both shuffled control data and individual 1-s time binned spike data (Ps < 0.001). × indicates the Sequence × Approach two-way interaction. Error bars: SEM. *** P < 0.001. ns: not significant.

DISCUSSION

Our findings revealed that neurons in the dorsomedial posterior parietal cortex (dmPPC) exhibit responses to an array of cinematic features. We demonstrated that dmPPC neurons showed mixed selectivity responses to different categories of ethograms and low-level visual features. The amount of information embedded within neuronal spiking sequences were modulated by the convergence of multiple representations which in turn contribute to the read-out of different

content-types. The processing of category and feature information by these neurons is sustained by accumulation of temporal information over a long timescale, corroborating its role at the apex of the cortical hierarchy of temporal receptive windows.

The neurons in the dmPPC demonstrate mixed selectivity representations to distinct features (e.g., aggressive behavior and allogroom) or combinations of dimensional features that appear sequentially over the course of dynamic videos, implying a flexible and efficient computational function of dmPPC in the processing of multiplex information in rich fast-changing environment (Fusi et al., 2016; Johnston et al., 2020; Murray et al., 2017). According to dual-process models in social cognition, the medial posterior parietal cortex is part of the reflective system corresponding to a controlled social cognition processing (Lieberman, 2007; Satpute & Lieberman, 2006). We hypothesize that the posterior parietal cortex plays an interface role in the integration of multifaceted information for social cognition. Neurons in dmPPC are consistently modulated by the observation of social interactions, such as inner group grooming behaviors (allogroom and scratch) and aggression performance (chase, strike, flee). Apart from Klein's observations that neuronal activity in primate LIP (lateral intraparietal) signaled values of conspecific genital cues (Klein et al., 2008), the modulation of neural activation is now also observed in dmPPC neurons in the present study, which could be accounted for by the inner anatomical connections in the posterior parietal lobe (Andersen et al., 1987; Leichnetz, 2001). Moreover, we observed that a large proportion of neurons respond to the presentation of foraging behaviors, which might be related to some previous findings that PGm (central precuneus) responds to observed and execution of reaching to grasp movement (Evangeliou et al., 2009). The neural modulation of these stimuli was likely due to the strong anatomical connections of Area 7 with PFG (Leichnetz, 2001) and suggests that this region shares the general function of visual spatial and action coding (Andersen, 1997; Andersen & Cui, 2009). We have now seen evidence suggesting that neurons in macaque's Area 7 express its intentions before actions (Snyder et al., 1997) and that Area 7 strongly responds to conspecific social interactions in comparison to non-social interactions by inanimate objects (Sliwa & Freiwald, 2017).

Our findings demonstrated that neurons in the monkey dmPPC accumulated mixed selectivity representations across the duration of video to support the construction of episodes, providing evidence that the PPC sustains a long temporal receptive window. Indeed, the dmPPC has been proposed to code information with long timescales (Hasson et al., 2015; Runyan et al., 2017). An fMRI study that presented movies to human participants reported that medial posterior parietal cortex (precuneus) accumulates information up to 12 s (Hasson et al., 2008). We argued that the long TRW allows the dmPPC to accumulate the continuous information of multifaceted representations from unimodal or integration of cross-modal inputs (Gilissen & Arckens, 2021) to support processing stream of past experiences for episode. This aligns with the higher temporal dynamics in the precuneus when remembering the unfolding of events that included a high density of experience units (Jeunehomme et al., 2022). Notably, the primate dmPPC has dense connections to the hippocampal formations in the primate (Kravitz et al., 2011). Given the known importance of schema cells in the primate hippocampus (Baraduc et al., 2019) and how such cells might code for information about space and nonspatial elements of the environment for both perceptual and mnemonic experiences (Gulli et al., 2020; Zhang et al., 2022), it is likely that the two structures support an information abstraction system that is driven by a broad range of behaviorally relevant inputs.

Indeed, the dmPPC is part of the posterior memory network (Ranganath & Ritchey, 2012). A recent study demonstrated that precuneal lesions impaired the time orientation as well as the damage of memory retrieval (Skye et al., 2022), implying that the dmPPC contribute to implementing and organizing transitions between experience units during memory formation and temporal unfolding of past events (Brodt et al., 2016; Foudil et al., 2020). Our neuronal results confirm prior findings that the temporal dynamics in the precuneus contribute to the processing of encoding remembered duration (Dušek et al., 2012), the representation of

temporal structure and order of moments of past events (Aly et al., 2018; Kwok et al., 2012), as well as the experience-based planning in the future (Madore et al., 2016). Considering that the homolog of our target brain region (Area 7a) between humans and monkeys is separated by a stark divergence of around 25 million years (Bruner et al., 2017), our current findings carry important insights into the neural correlates of the primordial form of our episodic processing ability.

Functional MRI studies using dynamic movie stimuli demonstrated that the medial PPC is involved in the motion information processing in both humans and monkeys (Bartels et al., 2008; Russ & Leopold, 2015). This is in line with our observation that neural activity in dmPPC were modulated by motion features, including optical flow (Raffi & Siegel, 2007) and motions caused by camera movement and animal appearance (count), aggressive behaviors (e.g., chase, strike, flee), and other features correlated with the fluctuations in early visual areas (Russ & Leopold, 2015). Neuronal responses to the convergence of multiplex dimensional stimuli suggest that dmPPC is involved in the integration of inputs from inner projections in the PPC (Andersen et al., 1987), from the early visual cortex (Robinson et al., 1978), and with the hippocampus (Baraduc et al., 2019; Gulli et al., 2020; Zhang et al., 2022).

Compared to static stimuli, the use of dynamic naturalistic videos, which meets the ethological validation from sensory to social cognition research (Adams et al., 2021; Mosher et al., 2014; Testard et al., 2021), helped us yield significant findings in the present study. We acknowledge that the analyses and their conclusions are based on correlational measures between action potentials and cognitive indices. In future work, micro-stimulation by electrical or targeted pharmacological intervention would be instrumental for a detailed elucidation of the complex cognitive roles carried out by the primate dorsomedial posterior parietal neurons.

STAR*METHODS

KEY RESOURCES TABLE

REAGENT or RESOURCE	SOURCE	IDENTIFIER
Chemicals, peptides, and recombinant proteins		
Tolfedine	Vetoquinol	N/A
Baytril	Bayer HealthCare LLC.	N/A
Zoletil	Virbac	N/A
Dexamethasone	Jilin Huamu Animal Health Products CO., Ltd.	N/A
Refine Bright	Yamahachi Dental MFG.CO.	N/A
Super Bond	Sun Medical Co., Ltd	N/A
Palacos	Heraeus Medical	N/A
Gadopentetate dimeglumine	Shanghai Xudong Haipu Pharmaceutical Co., Ltd	N/A
Glucose-saline	Sake-biotech	N/A
Experimental models: Organisms/strains		
Rhesus Macaque (*Macaca Mulatta*)	Beijing Institute of Xieerxin Biology Resource	http://www.xexbio.com/cn
Software and algorithms		
MATLAB	MathWorks Inc.	https://www.mathworks.com/
Horn-Schunk	N/A	https://www.mathworks.com/matlabcentral/fileexchange/22756-horn-schunck-optical-flow-method
Python 3.1.0	N/A	https://www.python.org/
OpenCV	N/A	Python package
PsychoPy 3.1.2	N/A	https://www.psychopy.org/
R 4.1.0	N/A	https://www.r-project.org/
glmnet	N/A	R package
Tinbergen Alpha	N/A	https://zenodo.org/record/13009#.YnKNs9pByiM
Offline Sorter 4	Plexon	https://plexon.com/products/offline-sorter/
NeuroExplorer 5	Plexon	https://plexon.com/products/neuroexplorer/
Video Studio X8	Corel Corporation	https://www.videostudiopro.com/
3D Slicer	N/A	https://www.slicer.org/
Gephi	NA	https://gephi.org/ (Bastian et al., 2009)
Other		
SC32	Gray Matter Research	N/A
Ceramic bone screws	Gray-Matter Research	N/A
Polyether-ether-ketone (PEEK)	Gray-Matter Research	N/A
LMA single shank	Microprobes	N/A
RHD2000	Intan Technologies	N/A
SmartBox	NeuroNexus Technologies Inc.	N/A
Microdrive	FHC Inc.	N/A
5-RLD-D1	Crist Instrument Co., Inc., U.S.	N/A
Eyelink 1000	SR Research	N/A

RESOURCE AVAILABILITY

Lead contact. Further information and requests for resources should be directed to the Lead Contact, Sze Chai Kwok (sze-chai.kwok@st-hughs.oxon.org).

Data and code availability. Raw electrophysiological data, analysis code, and processed data supporting the conclusions of this study are available upon request.

EXPERIMENTAL MODEL AND SUBJECT DETAILS

Subjects

Three male rhesus macaques (*Macaca mulatta*) (8.7 ± 0.46kg) with a mean age of 6.67 years old served as subjects in this study (monkey G: 8y, 9.2kg; monkey J: 6y, 8.3kg; monkey M: 6y, 8.6kg). All monkeys were single-housed with a 12:12 (7: 00am/7:00 pm) light-dark circle and kept within the temperature range of 18 - 23℃ and humidity between 60% - 80%. The animals were fed twice a day with each portion of at least 180g monkey chow and pieces of apple (8:30 am/4:00 pm). Water was limited during recording days. All animal care, experimental, surgical procedures, and pre/post surgical care were approved by the Institutional Animal Care and Use Committee (permission code: M020150902 & M020150902-2018) at East China Normal University.

Before this study, monkey J and monkey M participated in a temporal order judgment behavioral experiment (Wang et al., 2020; Zuo et al., 2020). Monkey G was trained on fixation and saccadic tasks and participated in several oculomotor studies while neuronal activities were recorded from right medial temporal (MT) and medial superior temporal (MST) areas using single-tetrode tungsten electrodes in a different study.

METHOD DETAILS

Experimental procedure and overview

During this study, the monkeys sat in a custom-manufactured Plexiglas monkey chair (29.4 cm × 30.8 cm × 55 cm) with a head-fixed (see **Surgery**) in front of a 19-inch screen (An-190W01CM, Shenzhen Anmite Technology Co, Ltd., China) which mounted on a stainless-steel platform. Monkeys' eyes are about 60 cm and 62 cm away from the screen's top edge and bottom edge, respectively. Water was delivered by a distributor (5-RLD-D1, Crist Instrument Co., Inc., U.S.) as a reward.

In each session, the monkeys watched 3 different 30-s video footage presented with PsychoPy (PsychoPy 3.1.2, PsychoPy), each for 30 repetitions arranged in 6 blocks. The same list was repeatedly presented in two consecutive days (12 days in total). Each video was watched 60 times. 15 videos were continuously and automatically displayed in each block for monkey J and monkey M. 1ml water was delivered at the beginning of each video, and following a 6-s blank period at the end of the video, another 1.8ml water was delivered.The monkeys took a 5-minute break between blocks (Figure S1A).

Experimental stimuli

The stimuli used in this study were downloaded from YouTube. Next, we applied Video Studio X8 (Corel Corporation, Canada) to edit these videos into 720P segments with 25 frames per second. In total, we prepared eighteen 30-s footage that were classified into three categories: 1) Primate content: with depictions of activities of monkeys; 2) Non-primate content: with activities of other species, including deers, lions, hippopotamus, hyenas, storks, rhinoceros, ostriches, penguins, and giraffes; 3) Scenery content: with depictions of dynamic naturalistic scenes without any animals.

Ethogram analysis

Ethogram is used to systematically describe a set of archetypal naturalistic behaviors by using descriptive terms and phrases of a species. For the collection of videos (see **Stimuli**), we constructed an inventory of behaviors by adapting the ethogram framework for macaque monkeys (Adams et al., 2021; Partan, 2002) and coordinating behaviors for non-primates displayed in used videos (Dinerstein, 2003; Gottschalk et al., 2019; Kahl, 1966; MacNulty et al., 2007; Sauer & Sauer, 1967; Seddon, 1991; Seeber et al., 2012; Stanton et al., 2015; Wark et al., 2019; Zhigang, 2006). The most common behaviors and related definitions of these distinctive animals presented in the videos were summarized in Table 2. The binary value of the time series of perceptible behaviors for each video was manually registered by Tinbergen (Adams, 2014).

Low-level features extraction

Measures of video low-level features were extracted by applying Python and MATLAB for further modeling (Figure S2A-S2C). OpenCV package (Bradski & Kaehler, 2000) was called in Python for the calculation of luminance, contrast, and saturation. Luminance of each video frame was the mean of the pixel-wise luminosity, which was computed with the following equation $l_{pixel} = 0.299 * R + 0.587 * G + 0.114 * B$ (Jack, 2008). Contrast of each frame was the standard deviation of the pixel-wise intensity distribution of the grayscale frame (Perfetto et al., 2020). Saturation was the mean pixel-wise S value of HSV color space that transformed from RGB color space (Jack, 2008). Motion was evaluated by the mean velocity magnitudes of optical flow by using the in-built Horn-Schunk algorithm in MATLAB (Bartels et al., 2008; Sliwa & Freiwald, 2017).

Electrophysiological recording and spike sorting

By using chronically implanted glass-coated electrodes from the right hemisphere (SC32, Gray Matter Research, LLC, USA;) on monkeys J and M, and by using single-wire tungsten microelectrode with 24 probes (LMA single shank, Microprobes, USA) on monkey G. In each recording session, the monkeys sat in chairs with their heads fixed. Headstage of multi-channel utility was connected to the SmartBox (NeuroNexus technologies, Inc., USA) acquisition system via an amplifier Intan adapter (RHD2000, Intan Technologies, USA) with 32 unipolar inputs. Microelectrodes impedance of each channel was in the range of 0.5 to 2.5 MΩ and measured at the beginning of the session. Spike waveforms above a set threshold were identified with a 1000 Hz online high-pass filter. Electrophysiological data collection was band-pass filtered from 0.1 to 5500 Hz and digitized at 30 kHz. Electrophysiological data from different sessions were treated as separate ones. Single units and their spikes were then identified based on peak amplitude, principal component, auto-correlation, and spike width by using Offline Sorter (Plexon Inc., USA). Units with an overall mean firing rate of fewer than 1 Hz across video presentations were excluded from further analysis.

Before recording, for monkeys J and M, channels without spikes were manually advanced anti-clockwise to detect promised spike waveform. On any given day, the individual electrode was advanced at most 8 rounds (1 mm) with the step of one-eighth to 1 round (15.625 to 125 μm). For monkey G, a custom-designed recording grid (Delrin, 56 mm × 33.5 mm, 5 mm in thickness) with interlaced holes (0.8 mm in diameter and 0.8 mm apart from each other) was fixed on the plastic chips in the head-post. Then, an accommodated guide tube leads the 24 probes tungsten microelectrode (LMA single shank, Microprobes, USA), with 0.1 mm spacing between adjacent probes, through the skull and dura. A hydraulic microdrive (FHC Inc., USA) was used to drive the microelectrode into the target cortex, which was determined by the fMRI image. By the end of the study, monkey J and M were imaged with CT, the location of each electrode was confirmed by mapping the CT image to fMRI T1 structures (Figure S1B). Histological recording sites were reconstructed based on the penetration depth of each electrode with the

chamber coordinates and angles to the transverse plane.

Surgical procedure for head-post and electrodes implantation

For monkeys J and M, the whole surgeries consisted of 2 stages: head-post installation and electrodes implantation. Each stage was followed by a recovery period during which one dose of analgesic (Tolfedine, Vetoquinol, New Zealand) and antibiotics (Baytril, Bayer HealthCare LLC., Germany) were daily given via intramuscular injection according to body weight for one week. All medical operations and health care pre-post surgeries comply with the Institutional Animal Care and Use Committee guidelines at East China Normal University.

Head-post installation. Food and water were limited to 12 h before surgery. Forty-five minutes before the surgery, one dose of atropine sulfate (Shanghai Pharma, Changzhou Pharmaceutical Factory Co., Ltd., China) was injected to reduce saliva secretion during operations. Ten minutes later, one dose of Zoletil (Zoletil, Virbac, New Zealand) was injected for anesthetization before monkeys were transferred to the preparation room for shaving the head skin. Once the skin was prepared, the monkeys were placed on the stereotaxic apparatus mounted on the operating table. A mixture of oxygen and isoflurane was inhaled with the help of a ventilator. Dexamethasone (0.5mg/kg, Jilin Huamu Animal Health Products CO., LTD, China) was administered via intravenous transfusion with a 5% glucose-saline (Sake-biotech, China) injection at the beginning of the surgery to reduce the intracranial pressure and avoid bone inflammation during or after the surgery. Respiration, heart rate, blood pressure, expired CO_2, and oxygen saturation were monitored during the whole surgical procedure. Body temperature was sustained at 37℃ with a constant temperature heater under the operating table. After successfully opening the epidermis and removing the subcutaneous tissues, an MRI-compatible polyether-ether-ketone (PEEK, Gray-Matter Research, Bozeman, USA) head post was cemented by acrylate cement (Refine Bright, Yamahachi Dental MFG.CO., Japan) which was then anchored with ceramic bone screws (Gray-Matter Research, Bozeman, USA) distributed on the anterior part of the skull. Sterilized saline was dropped to cool the hardened cement rapidly and clean the smoothed crumbs around the wound. Analgesics and anti-inflammatory were injected as required, when the ventilator was turned off and intravenous injection withdrew. MRI anatomical scans were acquired 4 months afterwards to aid subsequent implantation of the recording chambers.

Recording chamber implantation. Preoperative preparations were identical to the first stage. After opening the epidermis and removing the subcutaneous tissues, a craniotomy (5/8 inch in diameter) was manually drilled over the right hemisphere of the monkey, while the center of the chamber was pre-determined by the simulation of 3D Slicer (Kikinis et al., 2014). Next, the surface around the craniotomy was polished into a plane, and the medial wall was smoothed to only accommodate the chamber of the acquisition system. Then, 12 ceramic screws were placed for chamber fixation, and 2 stainless steel screws were anchored for grounding purposes. After that, the surrounding areas of the screws were tightly sealed with Super Bond (Sun Medical Co., Ltd., Japan), and the chamber was fixed with Palacos (Heraeus Medical, US) and acrylate cement.

Immediately after that, the monkey was transferred into an MRI scanner and imaged with a fiducial filled with gadopentetate dimeglumine (Shanghai Xudong Haipu Pharmaceutical Co., Ltd, China) that diluted 750 times. The center of the chamber was re-coordinated based on the modeling with fiducial marker by using 3D Slicer (monkey J: anterior-posterior (AP): -16.4 mm, medial-lateral (ML): 5.8 mm lateral to medial, 28° angle to the right and 14° angle to the posterior of the transverse plane; monkey M: AP: -15.422 mm, ML: 7.549 mm, 25° angle to the right and 9.1° angle to the posterior; Figure S1CB & 1C), covering paracentral of area 7a. Lastly, twenty-four hours later, the asepsis electrode-set was fitted into the chamber when monkeys were awake, and 44 rounds (5.5 mm) of each single electrode were gradually lowered anti-clockwise to penetrate through the dura and pia.

For monkey G, T1 images were scanned before surgery. After exposure of the skull and removal of the hypodermis, a lightweight acrylic cap was anchored by six titanium screws with acrylate cement for head-fixation. Then, the cavity of the chamber was filled with a layer of cement, and two custom-designed plastic chips (10 mm × 56 mm, 5 mm in thickness) were stabilized over the hardened cement for recording grid restriction. At the end of the surgery, an acrylic resin cap was covered over the chamber to keep inside free from pollution. The monkey was allowed to rest for recovery (Jia et al., 2021).

QUANTIFICATION AND STATISTICAL ANALYSIS

Data analysis was performed using custom software written in R, Python, and MATLAB.

Feature selection with LASSO regression

To evaluate the modulation of perceived behaviors to the neural activity, the 'glmnet' package (Friedman et al., 2017) in R language was employed to build a linear model with elastic net regulation LASSO (least absolute shrinkage and selection operator) feature selection algorithm (Tibshirani, 1996). In contrast to the commonly used general linear model, LASSO regression has advantages for the present study. Annotation of ethograms produced a schematic binary time-series with 52 dimensions embedded within all the videos. An important feature of the ethogram is that some items are linearly correlated. For example, if the count of animals is larger than 2, the animal count must be larger than 1. A large number of regressors and multi-collinearity of simultaneous happenings tend to cause overfitting, which will increase the value of cost function, and reduce the explanatory power of the model. The LASSO regression will scale all variables, and shrink coefficients of less important predictors to 0 to filter out these redundant items from the model. In short, the LASSO algorithm selects features with non-zero coefficients by minimizing the prediction error of the model (Muthukrishnan & Rohini, 2016; Tibshirani, 1996; Zou & Hastie, 2005), which allowed us to determine which selected feature modulates the neural activity.

For each neuron, we first concatenated the sequences of average superposed spike counts in 40 ms time-bin over 30 repetitions, as well as the time-series of ethograms, in the order of Non-primate, Primate, and Scenery video. A LASSO regression was constructed to model the modulation of 52 ethogram items and 4 low level features as variables on neuronal activity. With an increasing parameter λ, the algorithm iteratively penalized coefficients of all items gradually shrinking to zero (Figure S3A and S3B). An optimal λ was obtained by an in-built cross-validation procedure when the LASSO algorithm reached a minimum residual sum of squares. With the optimal λ parameter, these features with non-zero coefficients were then selected into the model (Figure S3C), implying that neural activity was effectively modulated by these selected features. Finally, for model validation, we performed a cross-validation with a model with features using random 80% of the sample data to predict the remaining 20% of the data. (Figure S3D).

Decoding Analysis

Content Discriminability. A support vector machine (SVM) classifier with a leave-one-out cross-validation approach was performed on trial spike counts sequence binned in 1 s bins to quantify the representations of categorical natural episodes within neuronal activity with the help of the 'e1071' (Meyer et al., 2019) package in R. For each neuron, a multi-class decoder was trained on 87 trials (29 trials of each video), and tested on left 3 trials using a one-versus-all method. Overall decoding performance was estimated as the average accuracy over 30 repetitions. At the same time, the decoding accuracy of each video content was taken as the percentage of trials correctly predicted. To test the significance of decoding ability, we trained a multi-class classifier using spike sequences with randomly shuffled labels of training data and tested the left shuffled-label trials over 1000 repetitions. The statistical significance of real

decoding performance was determined in comparison to the 95% percentile of shuffled decoding accuracy.

Temporal Accumulation. We iteratively trained the SVM decoder utilizing spike counts in 1 s time bins from the 1st to the 30th time bin for the temporal accumulation decoding analysis. A proposed leave-one-out cross-validation training-testing SVM decoding approach was implemented at each accumulation timepoint. Spike count in the 1st time-bin, for example, was used for the 1st accumulation timepoint. The spike count sequences from the 1st to 2nd time bins were used in the decoding technique for the 2nd accumulation timepoint, while sequences of spike count from the 1st, 2nd, and 3rd time bins were used in the decoding approach for the 3rd timepoint, and so on. We performed a similar decoding study for all individual timepoints to confirm that the accumulating effect is an intrinsic neural function rather than a momentary response activity to stimuli. For the estimation of statistical significance, a similar permutation SVM decoding technique was used for corresponding accumulation and individual timepoints, respectively.

We defined three criteria to verify the accumulation neuron; (1) decoding accuracy in real firing sequences is significantly higher than corresponding label-shuffled firing sequences; (2) decoding accuracy in real firing sequences is significantly higher than corresponding individual timepoint decoding performance; (3) decoding performances in real firing sequences as a function of accumulated time point.

Chi-squared simulation

A Chi-squared simulation procedure is used to determine the chance level of percentage of units modulated by specific selected features. The chance level is determined at 7.2% (or 27 /375 neurons, see dashed line in Figure 2B).

SUPPLEMENTAL INFORMATION

Supplemental information can be found online.

ACKNOWLEDGMENTS

This work received support from the National Natural Science Foundation of China (32071060), the Science and Technology Commission of Shanghai Municipality (201409002800), internal funding from School of Psychology and Cognitive Science (East China Normal University), and Jiangsu Qinglan Talent Program Award (SCK). We thank Emiliano Macaluso for his helpful comments on the manuscript.

AUTHOR CONTRIBUTIONS

Conceptualization, L.W., S.C.K.; methodology, L.W., M.K., S.C.K.; investigation, L.W., X.Z., J.Y., F.Z., S.Z.; formal analysis, L.W., X.Z., J.Y.; visualization, L.W.; writing – original draft, L.W.; writing – review & editing, L.W., M.K., Y-D.Z., H.M.W., A.C., S.C.K.; supervision, H.M.W., S.C.K.; funding acquisition, Y-D.Z, S.C.K..

DECLARATION OF INTERESTS

The authors declare no competing interests.

References

Adams, G. K., Ong, W. S., Pearson, J. M., Watson, K. K., & Platt, M. L. (2021). Neurons in primate prefrontal cortex signal valuable social information during natural viewing. *Philosophical Transactions of the Royal Society B*, *376*(1819), 20190666.

Aly, M., Chen, J., Turk-Browne, N. B., & Hasson, U. (2018). Learning naturalistic temporal structure in the posterior medial network. *Journal of Cognitive Neuroscience*, *30*(9), 1345-1365.

Andersen, R., Essick, G., & Siegel, R. (1987). Neurons of area 7 activated by both visual stimuli and oculomotor behavior. *Experimental Brain Research*, *67*(2), 316-322.

Andersen, R. A. (1997). Multimodal integration for the representation of space in the posterior parietal cortex. *Philosophical Transactions of the Royal Society of London. Series B: Biological Sciences*, *352*(1360), 1421-1428.

Andersen, R. A., & Cui, H. (2009). Intention, action planning, and decision making in parietal-frontal circuits. *Neuron*, *63*(5), 568-583.

Andric, M., Goldin-Meadow, S., Small, S. L., & Hasson, U. (2016). Repeated movie viewings produce similar local activity patterns but different network configurations. *Neuroimage*, *142*, 613-627.

Baraduc, P., Duhamel, J.-R., & Wirth, S. (2019). Schema cells in the macaque hippocampus. *Science*, *363*(6427), 635-639.

Bartels, A., Zeki, S., & Logothetis, N. K. (2008). Natural vision reveals regional specialization to local motion and to contrast-invariant, global flow in the human brain. *Cerebral cortex*, *18*(3), 705-717.

Bastian, M., Heymann, S., & Jacomy, M. (2009). Gephi: an open source software for exploring and manipulating networks. Proceedings of the international AAAI conference on web and social media,

Bradski, G., & Kaehler, A. (2000). OpenCV. *Dr. Dobb's journal of software tools*, *3*.

Brodt, S., Gais, S., Beck, J., Erb, M., Scheffler, K., & Schönauer, M. (2018). Fast track to the neocortex: A memory engram in the posterior parietal cortex. *Science*, *362*(6418), 1045-1048.

Brodt, S., Pöhlchen, D., Flanagin, V. L., Glasauer, S., Gais, S., & Schönauer, M. (2016). Rapid and independent memory formation in the parietal cortex. *Proceedings of the National Academy of Sciences*, *113*(46), 13251-13256.

Bruner, E., Preuss, T. M., Chen, X., & Rilling, J. K. (2017). Evidence for expansion of the precuneus in human evolution. *Brain Structure and Function*, *222*(2), 1053-1060.

Cavanna, A. E., & Trimble, M. R. (2006). The precuneus: a review of its functional anatomy and behavioural correlates. *Brain*, *129*(3), 564-583.

Clewett, D., DuBrow, S., & Davachi, L. (2019). Transcending time in the brain: How event memories are constructed from experience. *Hippocampus*, *29*(3), 162-183.

Dinerstein, E. (2003). Appendix E. A Profile of Rhinoceros Behavior. In *The Return of the Unicorns* (pp. 283-286). Columbia University Press.

Dušek, P., Jech, R., Sieger, T., Vymazal, J., Růžička, E., Wackermann, J., & Mueller, K. (2012). Abnormal activity in the precuneus during time perception in Parkinson's disease: an fMRI study. *PLoS one*, *7*(1), e29635.

Evangeliou, M. N., Raos, V., Galletti, C., & Savaki, H. E. (2009). Functional imaging of the parietal cortex during action execution and observation. *Cerebral cortex*, *19*(3), 624-639.

Foudil, S.-A., Kwok, S. C., & Macaluso, E. (2020). Context-dependent coding of temporal distance between cinematic events in the human precuneus. *Journal of Neuroscience*, *40*(10), 2129-2138.

Freedman, D. J., & Ibos, G. (2018). An integrative framework for sensory, motor, and cognitive functions of the posterior parietal cortex. *Neuron*, *97*(6), 1219-1234.

Friedman, J., Hastie, T., Simon, N., Tibshirani, R., Hastie, M. T., & Matrix, D. (2017). Package 'glmnet.'. *Journal of Statistical Software*, *33*(1), 1-22.

Fusi, S., Miller, E. K., & Rigotti, M. (2016). Why neurons mix: high dimensionality for higher

cognition. *Current opinion in neurobiology*, *37*, 66-74.

Gardner, E. P., Babu, K. S., Reitzen, S. D., Ghosh, S., Brown, A. S., Chen, J., Hall, A. L., Herzlinger, M. D., Kohlenstein, J. B., & Ro, J. Y. (2007). Neurophysiology of prehension. I. Posterior parietal cortex and object-oriented hand behaviors. *Journal of Neurophysiology*, *97*(1), 387-406.

Ghaem, O., Mellet, E., Crivello, F., Tzourio, N., Mazoyer, B., Berthoz, A., & Denis, M. (1997). Mental navigation along memorized routes activates the hippocampus, precuneus, and insula. *Neuroreport*, *8*(3), 739-744.

Gilissen, S. R., & Arckens, L. (2021). Posterior parietal cortex contributions to cross-modal brain plasticity upon sensory loss. *Current opinion in neurobiology*, *67*, 16-25.

Gottschalk, A., Linder, A. C., Lyhne, H., Langbak, M. G., & Jensen, T. H. (2019). Investigating Personality in Polar Bears Using the Concept of Behavioral Instability.

Gulli, R. A., Duong, L. R., Corrigan, B. W., Doucet, G., Williams, S., Fusi, S., & Martinez-Trujillo, J. C. (2020). Context-dependent representations of objects and space in the primate hippocampus during virtual navigation. *Nature neuroscience*, *23*(1), 103-112.

Harvey, B. M., Klein, B. P., Petridou, N., & Dumoulin, S. O. (2013). Topographic representation of numerosity in the human parietal cortex. *Science*, *341*(6150), 1123-1126.

Hasson, U., Chen, J., & Honey, C. J. (2015). Hierarchical process memory: memory as an integral component of information processing. *Trends in cognitive sciences*, *19*(6), 304-313.

Hasson, U., Yang, E., Vallines, I., Heeger, D. J., & Rubin, N. (2008). A hierarchy of temporal receptive windows in human cortex. *Journal of Neuroscience*, *28*(10), 2539-2550.

Honey, C. J., Thesen, T., Donner, T. H., Silbert, L. J., Carlson, C. E., Devinsky, O., Doyle, W. K., Rubin, N., Heeger, D. J., & Hasson, U. (2012). Slow cortical dynamics and the accumulation of information over long timescales. *Neuron*, *76*(2), 423-434.

Hutchinson, J. B., Uncapher, M. R., & Wagner, A. D. (2015). Increased functional connectivity between dorsal posterior parietal and ventral occipitotemporal cortex during uncertain memory decisions. *Neurobiology of learning and memory*, *117*, 71-83.

Jack, K. (2008). Color spaces. *Digital Video and DSP*, 15-29.

Jeunehomme, O., Heinen, R., Stawarczyk, D., Axmacher, N., & D'Argembeau, A. (2022). Representational dynamics of memories for real-life events. *BioRxiv*.

Jia, J., Puyang, Z., Wang, Q., Jin, X., & Chen, A. (2021). Dynamic encoding of saccade sequences in primate frontal eye field. *The Journal of Physiology*, *599*(22), 5061-5084.

Johnston, W. J., Palmer, S. E., & Freedman, D. J. (2020). Nonlinear mixed selectivity supports reliable neural computation. *PLOS computational biology*, *16*(2), e1007544.

Kahl, M. (1966). Comparative ethology of the Ciconiidae. Part 1. The marabou stork, Leptoptilos crumeniferus (Lesson). *Behaviour*, 76-106.

Kikinis, R., Pieper, S. D., & Vosburgh, K. G. (2014). 3D Slicer: a platform for subject-specific image analysis, visualization, and clinical support. In *Intraoperative imaging and image-guided therapy* (pp. 277-289). Springer.

Klein, J. T., Deaner, R. O., & Platt, M. L. (2008). Neural correlates of social target value in macaque parietal cortex. *Current Biology*, *18*(6), 419-424.

Kravitz, D. J., Saleem, K. S., Baker, C. I., & Mishkin, M. (2011). A new neural framework for visuospatial processing. *Nature Reviews Neuroscience*, *12*(4), 217-230.

Kwok, S. C., Shallice, T., & Macaluso, E. (2012). Functional anatomy of temporal organisation and domain-specificity of episodic memory retrieval. *Neuropsychologia*, *50*(12), 2943-2955.

Leichnetz, G. R. (2001). Connections of the medial posterior parietal cortex (area 7m) in the monkey. *The Anatomical Record: An Official Publication of the American Association of Anatomists*, *263*(2), 215-236.

Lieberman, M. D. (2007). Social cognitive neuroscience: a review of core processes. *Annu. Rev. Psychol.*, *58*, 259-289.

MacNulty, D. R., Mech, L. D., & Smith, D. W. (2007). A proposed ethogram of large-carnivore predatory behavior, exemplified by the wolf. *Journal of Mammalogy*, *88*(3), 595-605.

Madore, K. P., Szpunar, K. K., Addis, D. R., & Schacter, D. L. (2016). Episodic specificity induction impacts activity in a core brain network during construction of imagined future experiences. *Proceedings of the National Academy of Sciences*, *113*(38), 10696-10701.

Meyer, D., Dimitriadou, E., Hornik, K., Weingessel, A., Leisch, F., Chang, C.-C., Lin, C.-C., & Meyer, M. D. (2019). Package 'e1071'. *The R Journal*.

Morecraft, R., Cipolloni, P., Stilwell-Morecraft, K., Gedney, M., & Pandya, D. (2004). Cytoarchitecture and cortical connections of the posterior cingulate and adjacent somatosensory fields in the rhesus monkey. *Journal of Comparative Neurology*, *469*(1), 37-69.

Mosher, C. P., Zimmerman, P. E., & Gothard, K. M. (2014). Neurons in the monkey amygdala detect eye contact during naturalistic social interactions. *Current Biology*, *24*(20), 2459-2464.

Murray, J. D., Bernacchia, A., Freedman, D. J., Romo, R., Wallis, J. D., Cai, X., Padoa-Schioppa, C., Pasternak, T., Seo, H., & Lee, D. (2014). A hierarchy of intrinsic timescales across primate cortex. *Nature neuroscience*, *17*(12), 1661-1663.

Murray, J. D., Jaramillo, J., & Wang, X.-J. (2017). Working memory and decision-making in a frontoparietal circuit model. *Journal of Neuroscience*, *37*(50), 12167-12186.

Muthukrishnan, R., & Rohini, R. (2016). LASSO: a feature selection technique in predictive modeling for machine learning. 2016 IEEE international conference on advances in computer applications (ICACA),

Onoe, H., Komori, M., Onoe, K., Takechi, H., Tsukada, H., & Watanabe, Y. (2001). Cortical networks recruited for time perception: a monkey positron emission tomography (PET) study. *Neuroimage*, *13*(1), 37-45.

Partan, S. (2002). Single and multichannel signal composition: facial expressions and vocalizations of rhesus macaques (Macaca mulatta). *Behaviour*, *139*(8), 993-1027.

Perfetto, S., Wilder, J., & Walther, D. B. (2020). Effects of spatial frequency filtering choices on the perception of filtered images. *Vision*, *4*(2), 29.

Raffi, M., & Siegel, R. M. (2007). A functional architecture of optic flow in the inferior parietal lobule of the behaving monkey. *PLoS one*, *2*(2), e200.

Ranganath, C., & Ritchey, M. (2012). Two cortical systems for memory-guided behaviour. *Nature Reviews Neuroscience*, *13*(10), 713-726.

Reagh, Z. M., & Ranganath, C. (2021). A cortico-hippocampal scaffold for representing and recalling lifelike events. *BioRxiv*.

Rigotti, M., Barak, O., Warden, M. R., Wang, X.-J., Daw, N. D., Miller, E. K., & Fusi, S. (2013). The importance of mixed selectivity in complex cognitive tasks. *Nature*, *497*(7451), 585-590.

Robinson, D. L., Goldberg, M. E., & Stanton, G. B. (1978). Parietal association cortex in the primate: sensory mechanisms and behavioral modulations. *Journal of Neurophysiology*, *41*(4), 910-932.

Runyan, C. A., Piasini, E., Panzeri, S., & Harvey, C. D. (2017). Distinct timescales of population coding across cortex. *Nature*, *548*(7665), 92-96.

Russ, B. E., & Leopold, D. A. (2015). Functional MRI mapping of dynamic visual features during natural viewing in the macaque. *Neuroimage*, *109*, 84-94.

Satpute, A. B., & Lieberman, M. D. (2006). Integrating automatic and controlled processes into neurocognitive models of social cognition. *Brain research*, *1079*(1), 86-97.

Sauer, E. F., & Sauer, E. (1967). Yawning and other maintenance activities in the South African Ostrich. *The Auk*, 571-587.

Seddon, P. (1991). An ethogram for the Yelloweyed Penguin megadyptes antipodes. *Marine Ornithology*, *19*, 109-115.

Seeber, P. A., Ciofolo, I., & Ganswindt, A. (2012). Behavioural inventory of the giraffe (Giraffa camelopardalis). *BMC research notes*, *5*(1), 1-9.

Skye, J., Bruss, J., Herbet, G., Tranel, D., & Boes, A. D. (2022). Lesion Localization of Time Disorientation in Patients With Focal Brain Damage. *BioRxiv*.

Sliwa, J., & Freiwald, W. A. (2017). A dedicated network for social interaction processing in

the primate brain. *Science*, *356*(6339), 745-749.

Snyder, L. H., Batista, A., & Andersen, R. A. (1997). Coding of intention in the posterior parietal cortex. *Nature*, *386*(6621), 167-170.

Stanton, L. A., Sullivan, M. S., & Fazio, J. M. (2015). A standardized ethogram for the felidae: A tool for behavioral researchers. *Applied Animal Behaviour Science*, *173*, 3-16.

Testard, C., Tremblay, S., & Platt, M. (2021). From the field to the lab and back: neuroethology of primate social behavior. *Current opinion in neurobiology*, *68*, 76-83.

Tibshirani, R. (1996). Regression shrinkage and selection via the lasso. *Journal of the Royal Statistical Society: Series B (Methodological)*, *58*(1), 267-288.

Wallach, A., Melanson, A., Longtin, A., & Maler, L. (2021). Mixed selectivity coding of sensory and motor social signals in the thalamus of a weakly electric fish. *BioRxiv*.

Wang, L., Zuo, S., Cai, Y., Zhang, B., Wang, H., & Kwok, S. C. (2020). Fallacious reversal of event-order during recall reveals memory reconstruction in rhesus monkeys. *Behavioural Brain Research*, *394*, 112830.

Wark, J. D., Cronin, K. A., Niemann, T., Shender, M., Horrigan, A., Kao, A., & Ross, M. R. (2019). Monitoring the behavior and habitat use of animals to enhance welfare using the ZooMonitor app. *Anim. Behav. Cogn*, *6*, 158-167.

Zhang, B., Wang, F., Zhang, Q., & Naya, Y. (2022). Distinct networks coupled with parietal cortex for spatial representations inside and outside the visual field. *Neuroimage*, *252*, 119041.

Zhigang, J. (2006). Behavior coding and ethogram of the père david's deer. *Acta Theriologica Sinica*, *20*(1), 1.

Zou, H., & Hastie, T. (2005). Regularization and variable selection via the elastic net. *Journal of the royal statistical society: series B (statistical methodology)*, *67*(2), 301-320.

Zuo, S., Wang, L., Shin, J. H., Cai, Y., Zhang, B., Lee, S. W., Appiah, K., & Kwok, S. C. (2020). Behavioral evidence for memory replay of video episodes in the macaque. *Elife*, *9*, e54519.